TISSUE ENGINEERING: Part A
Volume 15, Number 7, 2009

DOI: 10.1089/ten.tea.2008.0238

In Vitro Evaluation of Macroporous Hydrogels to Facilitate Stem Cell Infiltration, Growth, and Mineralization

Vandana Keskar, B.S.,[1] Nicholas W. Marion, Ph.D.,[2] Jeremy J. Mao, D.D.S., Ph.D.,[2,*] and Richard A. Gemeinhart, Ph.D.[1,2]

Hydrogels have gained acceptance as biomaterials in a wide range of applications, including pharmaceutical formulations, drug delivery, and tissue sealants. However, exploiting the potential of hydrogels as scaffolds for cell transplantation, tissue engineering, and regenerative medicine still remains a challenge due to, in part, scaffold design limitations. Here, we describe a highly interconnected, macroporous poly(ethylene glycol) diacrylate hydrogel scaffold, with pores ranging from 100 to 600 μm. The scaffold exhibits rapid cell uptake and cell seeding without the need of any external force or device with high incorporation efficiency. When human mesenchymal stem cells are seeded within the porous scaffolds, the scaffolds were found to promote long-term stem cell viability, and on exposure to osteogenic medium, elicit an mineralization response as evaluated by an increased alkaline phosphatase activity (per cell) and calcium and phosphate content within the constructs. The atomic composition of the mineralized matrix was further determined by energy dispersive spectroscopy and found to be similar to calcium-deficient hydroxyapatite, the amorphous biological precursor of bone. The macroporous design of the hydrogel appears advantageous over similar porous hydrogel scaffolds with respect to ease of synthesis, ease of stem cell seeding, and its ability to support long-term stem cell survival and possible differentiation.

Introduction

An estimated 500,000 bone graft procedures were performed in the United States and one million worldwide in 2004.[1] Conditions that require bone graft procedures may be as varied as nonunion fractures, spinal fusions, craniofacial reconstruction, trauma, repair of bone voids after tumor resection, degenerative disorders, dental reconstruction, or instability problems involving joints in the upper and lower extremities.[2] Bone repair by autologous bone grafts would eliminate the problems of limited donor tissue availability, risk of disease transmission, and graft rejection. Traditional bone grafting involving autologous transplants is limited due to several reasons, including additional surgery to remove bone from the patient's own body, donor site morbidity, infection, and, above all, limited amount of healthy bone tissue that may be available. These realities make alternative therapeutic strategies attractive. Tissue engineering, which applies the principles of biology and engineering to the development of functional substitutes for damaged tissues or organs,[3] has the potential to overcome shortcomings of autologous and allogenic transplants by providing new materials as grafts for implantation. To achieve an effective tissue-engineered bone, appropriate scaffolds must be designed. In this work, we begin to examine a scaffold design based upon hydrogels that builds upon current scaffold design requirements.

In recent years, hydrogels have drawn a great deal of interest in the pharmaceutical and biomaterials fields mainly due to an inherent hydrated architecture that imparts mechanical properties similar to soft tissues and extracellular matrix.[4] Poly(ethylene glycol) diacrylate (PEGDA) hydrogels, in particular, have been widely investigated due to their hydrophilicity, favorable biological recognition properties, and ability to encapsulate cells within the hydrated network.[5,6] The nonadhesive nature of hydrophilic PEGDA hydrogels, due to poor protein adsorption to the surface, is generally thought to be unsuitable for anchorage-dependant cells to adhere directly. Therefore, modifications via incorporation of cell adhesive peptides, such as Arg-Gly-Asp (RGD), have been shown to overcome this limitation if sufficient and appropriate peptides are incorporated.[7,8] Both *in vitro* and *in vivo*, PEGDA hydrogels support mesenchymal stem cell (MSC) growth and differentiation toward bone,[6] cartilage,[9] and adipocytes[10] when cells are encapsulated directly within the slowly degrading hydrogel network. However, current PEGDA hydrogels are limited by this nonporous scaffold design and other factors. Macroscopic,

Departments of [1]Biopharmaceutical Sciences and [2]Bioengineering, University of Illinois, Chicago, Illinois.
*Present Address: College of Dental Medicine, Columbia University, New York, New York.

nonporous hydrogels, typically prepared by photopolymerization techniques, have the disadvantages of photoinitiator toxicity,[11] limited diffusion, and limited cell–cell interactions within the scaffolds.[12]

In comparison, porous scaffolds with a pore size of greater than 100 μm are reported to promote bone ingrowth within the pores of the scaffolds[13] and promote cell–cell interactions. Insufficient interconnectivity in biodegradable hydrophobic polymers, for example, poly(lactide-co-glycolide) copolymers, has been shown to be the limiting factor in cell colonization and new tissue formation,[14,15] but little is known concerning cellular infiltration or survival in porous hydrogel scaffolds. In a recent study, microchannel conduits were engineered in nonporous PEGDA hydrogels (NPHs) for generating vascularized adipose tissue grafts.[16] This study highlighted the necessity of a porous scaffold structure for vascularization. The presence of interconnected pores within the scaffold were shown to enable vascular capillary ingrowth from the host tissue into the interconnected network of the scaffold.[17] With this in mind, we hypothesized that three-dimensional (3D) superporous hydrogel (SPH)[18] scaffolds could be used to take advantage of the positive hydrogel attributes while addressing the issues known to exist with conventional hydrogel scaffolds.

SPHs are a class of macroporous hydrogels developed for fast-swelling applications.[18] SPHs can be prepared from addition monomers, such as PEGDA, by a gas foaming technique, wherein the foaming and gelation processes are simultaneous to yield hydrogels with a macroporous network. Due to this methodology, SPHs have a highly porous interconnected structure and large surface-to-volume ratio throughout the scaffold.[18] The gas foaming technique allows creation of a 3D porous structure without the use of organic solvents or a salt leaching step and without any limitations of scaffold thicknesses, drawbacks of the salt leaching and particulate leaching techniques currently employed for creation of macroporous architectures.[19]

The porous structure of the SPH was proposed to have ease of seeding of cell types, namely, human MSCs (hMSCs). Use of hMSCs was thought to be a promising strategy as hMSCs can be readily harvested from bone marrow aspirates from the patient. Bone marrow is the most enriched, easily accessible, and frequently used source from which MSCs can be easily isolated, expanded, and differentiated *in vitro*.[20–22] This presents the opportunity of using MSCs for autologous personalized therapy. Under the appropriate conditions, hMSCs have been shown to differentiate into multiple cell lineages that resemble osteoblasts, chondrocytes, and adipocytes.[22] MSCs can also differentiate into nonmesenchymal cells such as pulmonary epithelium,[23] kidney epithelium,[24] myocytes,[25] cardiomyocytes,[26] and neuronal cells.[27] MSCs have been successfully used to aid the healing of critical-sized skeletal defects in many animal models, including mice, rats, rabbits, swine, goats, and sheep.[2] Additionally, use of allogenic MSCs for repair of bone defects can be done without immunosuppressive therapy because MSCs do not express MHC class II molecules required to fully activate T cells responsible for graft rejection.[28] Because MSCs account for a very small fraction of the total population of nucleated cells (0.001–0.01%) within the marrow,[22] the *ex vivo* expansion of the number of stem cells followed by addition of growth factors to raise the osteogenic potential has been necessary for timely healing. *In vitro* osteogenic expansion and differentiation of MSCs has been well studied.[22,29–31]

With the knowledge of hydrogels as scaffolds and MSCs as a regenerative cell source that may need *ex vivo* expansion and/or differentiation, this study was designed to examine a macroporous scaffold with interconnected pores *in vitro*. Our specific objectives were to show rapid cell uptake within the scaffold, to show survival *in vitro* within the macroporous scaffolds over time, and to demonstrate the potential of the scaffold to support osteogenic mineralization of MSCs *in vitro*. Based upon the observations made in this study, further investigation and implantation with predifferentiated constructs and undifferentiated constructs are planned.

Materials and Methods

Preparation of macroporous PEGDA hydrogels

All chemicals were purchased as reagent grade and used without purification unless otherwise indicated. PEGDA ($M_n = 3400$ g/mol) was obtained commercially from Nektar (Huntsville, AL). To make the PEGDA SPH, PEGDA solution (15 [w/v]%), foam stabilizer (Pluronic® F127, Sigma, St. Louis, MO; 0.6 [w/v]%), double-distilled water, the initiator pair, *N*,*N*,*N*′,*N*′-tetramethylethylene-diamine (0.9 [v/v]%), and ammonium persulfate (0.7 [w/v]%) were added sequentially to a 4 mL glass vial ($d = 1.25$ mm; $h = 6$ mm) with the concentrations reported being the final concentration in the vial. Due to the configuration, the final formed SPH had a macroscopic morphology described by a right circular cylinder. Saturated citric acid solution was used to adjust the pH to 3.70. The precursor solution was mixed and heated gently to 37°C for approximately 2 min. Sodium bicarbonate, 200 mg, was added with constant stirring to evenly distribute the salt and evolving gas. Polymerization was allowed to proceed for half an hour. The SPHs were then removed from the vial and allowed to swell in double-distilled water to remove traces of unpolymerized monomers and salt before dehydrating in 80% ethanol followed by overnight dehydration in absolute ethanol. The hydrogels were then dried in a food desiccator and stored in an airtight container for further use.

To make the NPH, sodium bicarbonate, 200 mg, was replaced with sodium hydroxide solution (20 μL; 10 M). The precursor solution was pipetted into 96-well plates with each well containing an equivalent volume to the size of the total volume of the porous hydrogel. Polymerization was allowed to proceed for half an hour. The NPHs were then rinsed with double-distilled water to remove traces of unpolymerized monomers, dried, and stored in an airtight container for further use.

Cell adhesive peptides with integrin-binding sequence, acryl-GRGDSG (RGD), and a scrambled sequence, acryl-GDGRSG (DGR) as a control,[32] were dissolved in the precursor solution at a concentration of 2.5 mM and the remaining procedure for hydrogel preparation followed to give adhesive RGD-PEGDA SPHs and the expectedly nonadhesive DGR-PEGDA SPHs, respectively. Acryl-GRGDSG and acryl-GDGRSG peptide sequences were custom synthesized by solid-phase peptide synthesis (Protein Research Laboratory, University of Illinois at Chicago, IL) where acryl-G indicates an acrylated group added to the amino terminal using succinimide chemistry. The concentration of 2.5 mM

was chosen based upon the previously reported capacity of PEGDA hydrogels containing 1.25–2.5 mM RGD peptide within the hydrogels to promote osteogenesis in MSCs.[29] Incorporation of the peptides within the hydrogel was determined using fluorescein-conjugated versions of the peptides and found be 67–70% by fluorescent spectroscopy and confirmed by mass spectrometry. At this incorporation level (1.67–1.75 mM), the RGD density would correspond to 1.675 pmol RGD/cm^2—as determined for 10 nm of the hydrogel surface being available for interaction with cells[33]—which is well above the biologically relevant RGD density of 1 fmol RGD/cm^2 required for cell spreading and 10 fmol RGD/cm^2 that is reported to be required for formation of focal adhesion[34] although this is expected to vary for different cell types.

Equilibrium swelling measurements

Dried SPHs were cut to give final SPH of 5 mm diameter and 3 mm length (corresponding to approximately 59 μL, hereby referred to as simply SPHs). A beaker filled with 200 mL of phosphate-buffered saline (PBS; pH 7.4) was maintained at 37°C. Samples were weighed and added to the PBS. At specific time points, the swelling SPH was removed from PBS and blotted using paper towels to remove excess water from the surface and the pore network. The weight was recorded, and the sample returned to the beaker. Relative swelling ratio was calculated as the ratio of the swollen weight to the initial weight.

Distribution of cells seeded within PEGDA hydrogels

Cell suspensions of known cell density were added dropwise to each of the SPHs. Immediately after cell seeding, the cell-seeded hydrogels were placed in the incubator for 15 min to allow swelling equilibration. The distribution of cells within the hydrogels was observed by sectioning each hydrogel into three equal discs along the height with a scalpel. Each of the three discs was stained with the Live/Dead Viability/Cytotoxicity kit (Molecular Probes, Carlsbad, CA). Viable cells fluoresce green due to the cleavage of acetomethoxy-calcein (calcein AM) by intracellular esterases,[35] while nonviable cells fluoresce red due to the binding of ethidium homodimer to the nucleic acids that occurs due to loss of cell membrane integrity.[36] Images were taken from various locations and focal planes within the discs.

To further investigate the distribution of cells within the SPHs, NIH/3T3 cells (ATCC, CRL-1658) were seeded within SPHs using the same procedure. After 12 h of incubation, the SPHs are fixed in 10% buffered formalin and processed for paraffin embedding. The SPHs were sectioned into 5 μm cross sections (creating circular sections) with sections retained at 250 μm intervals along the axis of the cylinder. After sectioning, slides were stained with hematoxylin and eosin. Bright field images were taken to view the position of seeded cells within the SPH.

Finally, NIH/3T3 cells were loaded as described. The cylindrical SPHs were sectioned along their height into two symmetric cylinders with a scalpel. The top and bottom discs were further divided into four symmetric sectors each described by a subtended angle of 90°; thus, eight symmetric sections were created. The number of cells within each section was determined using the modified 3-(4,5-dimethylthiazol-2-yl)-2,5-diphenyltetrazolium bromide (MTT) assay[37] (Cell-Titer 96 Proliferation kit; Promega, Madison, WI) based upon a standard curve for these cells (data not shown). Briefly, a standard curve was obtained for cells seeded within the SPH versus the absorbance. For the standard curve development, cells were counted (Beckman-Coulter Multisizer™ 3 Coulter Counter®, Fullerton, CA), and serial dilutions were used to create cell suspensions in Dulbecco's phosphate-buffered saline with calcium and magnesium (DPBS) over a range of cell numbers in the presence and absence of hydrogels.

MSC isolation and seeding

hMSCs were isolated from whole bone marrow aspirates as previously reported.[10] MSCs from two different donors, up to passage 4, were used for all the experiments. For cell seeding, the SPHs were placed in 48-well plates. The MSCs were harvested using 0.25% trypsin with 1 M ethylenediaminetetraacetic acid, centrifuged, and resuspended in basal medium. This cell suspension, corresponding to a final cell number of 2.5×10^5 cells in approximately 40 μL of medium, was then added drop-wise to each of the SPHs. The hydrogels were placed in the incubator for 15 min to allow equilibrium swelling. Thereafter, 1 mL of corresponding medium was added to each of the wells, and the plates were incubated at 37°C in 5% CO_2. Basal medium consisted of Dulbecco's modified Eagle's medium (DMEM) supplemented with 10% fetal bovine serum, 100 units/mL penicillin, and 100 μg/mL streptomycin. Osteogenic medium consisted of basal medium with 100 nM dexamethasone, 10 mM β-glycerophosphate, and 0.05 mM ascorbic acid 2-phosphate.[22] Osteogenic medium treatment was started 24 h postseeding.

Cell viability within PEGDA hydrogels

MSC viability, measured as a function of mitochondrial activity, was determined by modified MTT assay as previously described. The SPHs were placed in a 48-well plate, and cell suspensions at appropriate cell density were seeded dropwise onto the SPHs. The volume of DPBS used to prepare the cell suspensions was normalized for all the cell densities. To every well, 200 μL of DPBS and 40 μL of reagent were then added directly. The plates were covered and incubated at 37°C for 2 h. At the end of 2 h, 100 μL of the supernatant was transferred to a new plate and read at a wavelength of 490 nm (Labsystems Multiskan Plate Reader, Golden Valley, MN). A standard curve (Fig. 1) was obtained by plotting the linear relationship between the cell number seeded and the absorbance value obtained. The controls for background absorbance were acellular SPHs in DPBS and empty wells.

To determine the incorporation efficiency within the SPHs immediately after seeding, the SPH were transferred to new well plates to exclude any cells that were not intimately interacting with the surface or entrapped within the SPH. The remainder of the procedure for the assay was as described above. Incorporation efficiency (%) was calculated as the absorbance of the sample divided by absorbance of the standard (cells added directly to the SPH and not moved to a new multiwell plate) multiplied by 100.

For determining the viability of cells seeded within the SPHs at various time intervals, the hydrogel samples were transferred to new multiwell plates—to remove cells

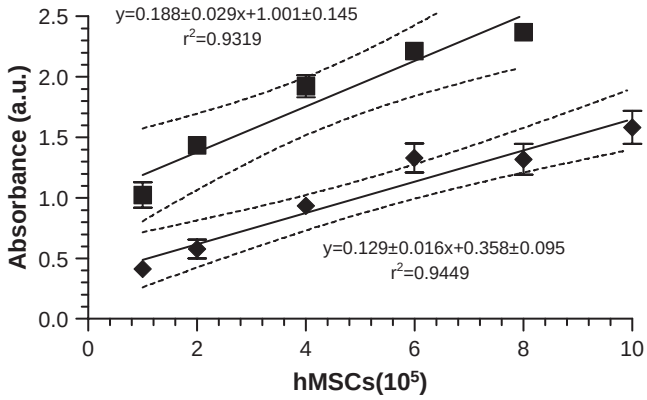

FIG. 1. Standard curve for MSCs seeded within PEGDA SPHs (◆) and on tissue culture plastic (■) using the modified MTT assay. Values are presented as mean ± standard deviation ($n = 3$). The solid lines represent the linear regression, and the dotted lines represent the 95% confidence limits of the linear regression. The slopes are similar ($p = 0.09869$), but the y-intercepts are significantly different ($p < 0.0001$).

adherent to the plate—and rinsed with DPBS to remove any serum components. Each SPH was then incubated with 200 μL of DPBS and 40 μL of reagent for 2 h, at the end of which 100 μL of the supernatant was transferred to a new plate and absorbance determined. Based on the standard curve previously obtained, the corresponding cell number for a given absorbance was determined.

At various time points, cell stains were used to visualize the cells within the pores of the hydrogels. Calcein AM was used to visualize live cells.[35] Actin staining[38] was achieved by fixing cells with 4% paraformaldehyde followed by staining with Alexa Fluor 546 phalloidin® (Molecular Probes, Carlsbad, CA), and Hoechst 33258 dye was used to visualize the nucleus.[39]

Human umbilical vein endothelial cells seeding and viability

Human umbilical vein endothelial cells (HUVECs) (BD™ Biosciences, San Jose, CA) were cultured in endothelial cell growth medium at 37°C in 5% CO_2 and used between passages 1 and 5. The procedures for cell seeding and cell viability measurements were similar as those for described for MSCs. A standard curve with HUVECs was also developed.

In vitro *mineralization*

Hydrogels were transferred to serum-free medium 24 h before collection to minimize serum components present within the hydrogels. Alkaline phosphatase (ALP) levels were determined by the formation of *p*-nitrophenol,[40] and was performed as per manufacturer's protocol (QuantiChrom™ Alkaline Phosphatase assay kit; BioAssay Systems, Hayward, CA). Calcium was determined by complexation of calcium by a phenolsulfonephtalein dye[41] (QuantiChrom Calcium assay kit; BioAssay Systems). Briefly, the lyophilized hydrogels were homogenized with 1 mL of 0.5 N HCl and mixed overnight at 4°C. The supernatant was used for calcium assays per manufacturer's protocol. Separate hydrogels were fixed with 4% paraformaldehyde, and the von Kossa staining technique[42] was used to visualize matrix mineralization.

Scanning electron microscopy and energy dispersive spectroscopy

Dried hydrogel samples were cut using a scalpel, and dehydrated. Energy dispersive X-ray spectroscopy (EDS; Oxford Inca, Elk Grove Village, IL) was performed on sections of the dried hydrogels taken from different locations within the porous structure of the SPHs to study the atomic composition of the deposited calcium. At least nine random locations in three independent SPHs were examined for each SPH and condition. After EDS analysis, samples were sputter coated with gold/palladium for scanning electron microscopy (SEM; Hitachi S-3000 N, Los Angeles, CA) imaging. SEM was used to investigate surface and interior morphology of the dried sections. Using MATLAB 6.1 (The MathWorks, Natick, MA), the SEM image was transformed to a binary image with the isodata threshold algorithm,[43] which calculates the best threshold value out of the gray-value histogram of the image. The binary image had two phases: the solid phase consisting of the hydrogel scaffold and the pore phase. Porosity was calculated as the ratio of the total number of pixels in the pore phase to the total number of pixels in the entire image. SEM images of dried section were used to gather information on the pore size distribution. To obtain the pore size distribution within hydrated SPHs, dried hydrogel sections were hydrated with PBS and allowed to swell to equilibrium after which the hydrated section was gently tapped on paper towels to remove excess PBS and observed under bright field. Images were used measure pore size within a fully hydrated SPH.

Data analysis

All data were expressed as a mean ± standard deviation and were compared using one-way ANOVA with subsequent *post hoc* test. Differences at *p*-value less than or equal to 0.05 were considered to be statistically significant. Finally, all error bars were presented as standard deviations.

Results

Pore structure and porosity measurements

The interior surface of the dehydrated SPH contained interconnected pores ranging from 100 to 600 μm (Fig. 2). The porosity of the SPHs was found to be 71 ± 2.1%. The pore size range of the hydrated SPH, estimated from bright field images, was within the same range, but slightly larger pores were observed (Fig. 2c). There was a broad distribution in the pore size with the hydrated SPHs having a larger pore diameter and broader distribution in pore diameter, 395 ± 107 μm, than the dehydrated SPH, 250 ± 94 μm. These sizes are similar to those previously reported for SPHs in both the dehydrated and hydrated states.[44] The swelling was rapid and reached equilibrium in PBS within seconds (Fig. 3). SPHs swelled to 90% of equilibrium weight within 3 min, indicating that the macro-

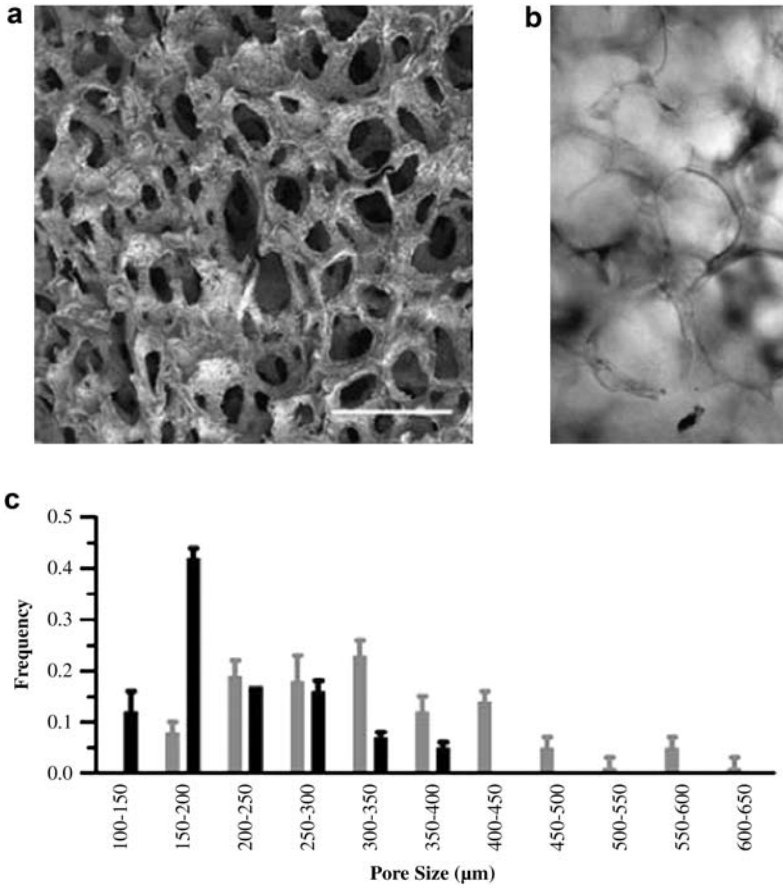

FIG. 2. Interconnecting pores can be seen where each pore was internally connected to the adjacent pores. (**a**) Representative scanning electron micrograph of the interior of dried PEGDA SPHs with scale bar of 500 μm. (**b**) Representative light micrograph of the interior of a hydrated PEGDA SPH with a scale bar of 500 μm. (**c**) Pore size distribution within dehydrated SPH (black bars) calculated from SEM micrographs and the SPHs that have attained equilibrium swelling (gray bars) calculated from light micrographs (average ± standard deviation; $n = 3$ hydrogels, and $n \geq 20$ pores).

porous structure is highly interconnected. This swelling is related to the filling of the pores followed by hydrogel swelling.[18] The interconnected nature of the pores and rapid pore filling was expected to contribute to uniform distribution of cells within the SPH.

Cell seeding and distribution within PEGDA hydrogels

After cell seeding within the SPHs by drop-wise addition of cell suspension to the dehydrated hydrogels (Fig. 3b), MSC incorporation efficiency was found to be $89 \pm 3.5\%$ of the total number of cells that were dropped onto the scaffold. The method of cell seeding employed was capable of delivering cells throughout the SPH (Fig. 4). The cells were all viable, and few (no more than five per frame of view) dead (membrane disrupted) cells were observed immediately after seeding (Fig. 4). MSCs were distributed widely in each of the sections with qualitatively similar distribution.

To support this, NIH/3T3 cells were observed across a full radial section at the axial center of an SPH. Cells were present throughout the section and at the very center of the SPH (Fig. 5). Qualitatively, the cells appear to be randomly distributed; however, there appeared to be nonhomogeneous distribution in the sections. This needs to be confirmed by more detailed localization experiments in the future, but the results clearly show that there are cells present in the interior and throughout the SPH immediately after seeding. To gain some quantitative understanding of the distribution of cells within the SPHS, eight sectors (four from the top half of the SPH and four from the bottom) were examined for uniformity of loading (Table 1). Depending upon the exact loading conditions, the sections were found to be statistically equivalent ($p = 0.069$).

MSC survival and viability within the pores of PEGDA hydrogels

Cells penetrated into the interior of the SPHs and concentrated around the edges of the pores within the SPHs (Fig. 6a; Supplemental Video S1, available online at www.liebertonline.com/ten). The hMSCs appeared to attach to the hydrogel and stained positive for the presence of actin filaments (Fig. 6b), suggesting cell–matrix interactions. While cells seeded within the pores of the PEGDA SPHs were seen present with native, spread morphology, cells seeded on top of nonporous, unmodified PEGDA hydrogels did not survive culture or populate the hydrogel surfaces (Fig. 6c). In comparison, RGD-modified PEGDA NPHs, as expected, enabled stem cell survival (Figs. 6d and 7). Within the PEGDA SPHs, cells were viable for a period of over 30 days. Interestingly, no significant difference was observed between the capacity of PEGDA SPHs and adhesive RGD-PEGDA SPHs to support stem cell growth (Fig. 7). MSCs grown on the RGD-containing NPH were able to maintain a high cell count, while MSCs on peptide-free NPH rapidly died.

The cell number was determined using the linearity of the modified MTT assay (Fig. 1) for the range of cells seeding used in this study. Similar standard curves were obtained for NIH/3T3 cells and HUVECs seeded within the pores of

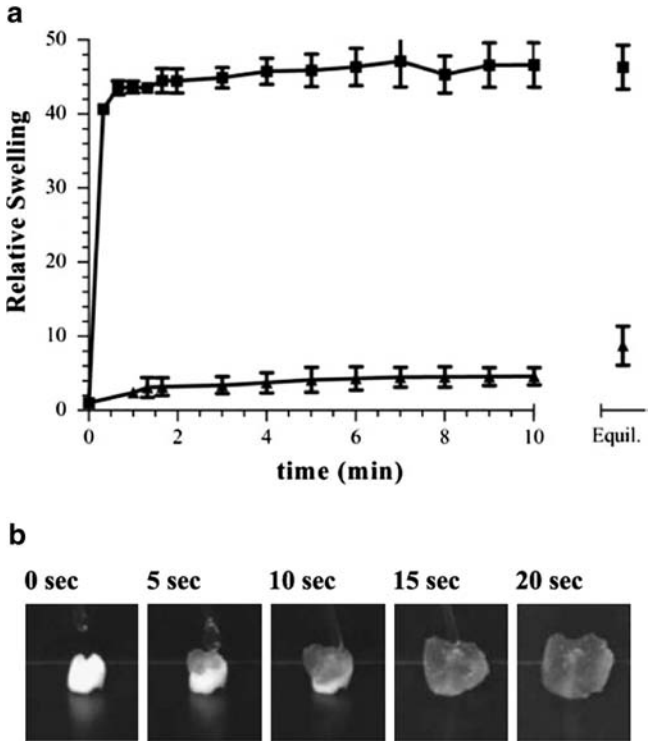

FIG. 3. (**a**) Relative swelling ratio of (■) SPHs and (▲) NPHs. The final point is at equilibrium (Equil.) at least 1 day after swelling began ($n = 3$; average ± standard deviation). (**b**) Real-time images of cell seeding within the SPH. A Pasteur pipette was used to drop cell suspension in DMEM.

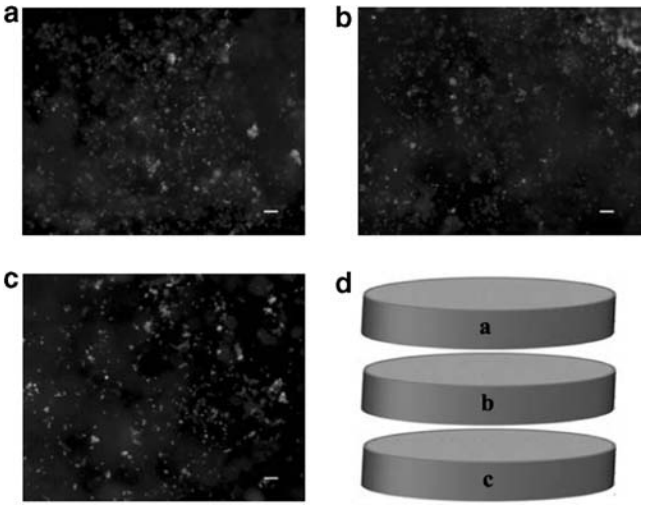

FIG. 4. MSC viability immediately upon seeding within the SPH. Viable cells (calcein AM) are observed throughout the SPHs, while few dead cells (not shown) are observed. Viable MSCs can be seen throughout the top (**a**), middle (**b**), and bottom (**c**) sections of the SPH at locations near the center (axial and radial) of each of the sections as depicted in (**d**). The scale bar is 100 μm in each image.

PEGDA SPHs, with R^2 values of 0.93 and 0.97, respectively (data not shown). Unlike DNA quantification methods that do not discriminate between DNA from dead cells or live cells,[45] the modified MTT assay is a cell viability assay and a more accurate predictor of the number of cells within the SPH that are available for further populating the SPH. Interestingly, cells were also encapsulated within PEGDA hydrogels and PEGDA SPHs, and no correlation was obtained between modified MTT absorbance and cell number at time points ranging from immediately after encapsulation to 48 h (data not shown).

HUVECs survival within PEGDA hydrogels

Unlike the hMSCs, which remained viable within unmodified PEGDA SPHs, HUVECs needed the adhesive RGD peptide for survival within SPHs (Fig. 8). HUVECs seeded on RGD-PEGDA SPHs proliferated to a relative cell count 69.8 ± 4.5% greater than seeded, while HUVECs seeded upon PEGDA SPHs and DGR-PEGDA SPHs did not survive with a relative cell count drop to 11.98 ± 1.63% ($p < 0.01$ compared to RGD-PEGDA NPH) and 7.87 ± 0.5% ($p < 0.0001$ compared to RGD-PEGDA NPH), respectively, of the seeded cells. This observation was not only in agreement with behavior of HUVECs on modified polymers,[46] but also confirmed that the cell adhesive peptides incorporated within the PEGDA SPHs were biologically active.

In vitro *mineralization*

PEGDA SPH (P), RGD-PEGDA SPH (R), and DGR-PEGDA SPH (D) cell-seeded constructs were cultured in DMEM basal medium (B) and osteogenic medium (O). Cells within the SPHs, upon exposure to osteogenic medium or basal medium, remained viable over the entire duration of the study (Fig. 9). Even after 7 weeks of culture, the cells were found concentrated around the pores (*) and throughout the porous structure (Fig. 9b). Gross visible calcification could be observed by the end of week 3, and by week 7 the

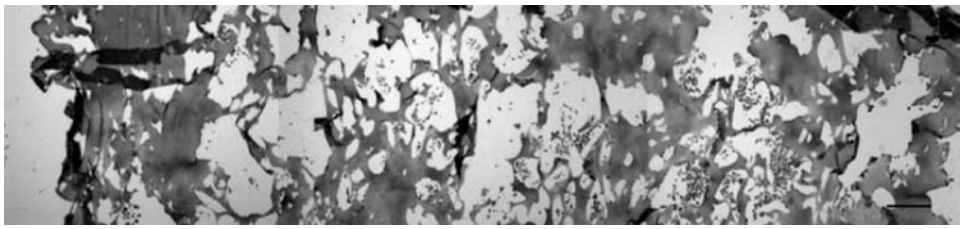

FIG. 5. Gray-scale micrograph of hematoxylin and eosin–stained NIH/3T3 cells within a 5 μm section of SPH collected 1250 μm below upper edge of the SPH. Cells can be seen throughout the representative stained section composed of three overlapping images taken to cover the entire SPH, edge to edge. The scale bar is 100 μm.

Table 1. Distribution of NIH/3T3 Fibroblasts in Eight Sections of a SPH

	Percent of the total cells loaded (mean ± standard deviation %)			
	1	*2*	*3*	*4*
Top	13.32 ± 1.96	11.31 ± 0.73	12.31 ± 2.08	10.18 ± 0.40
Bottom	14.58 ± 1.57	12.68 ± 1.16	12.76 ± 1.39	12.86 ± 1.60

Cells (7.5×10^5 cells) were seeded on the top of the hydrogel by drop-wise addition in approximately 40 μL of cell suspension ($n=3$, $p=0.069$). Each cylindrical hydrogel was cut in half by height, and each half of the SPH further sectioned into four identical radial sections.

exterior of the osteogenic samples was predominantly white from mineralization (Fig. 10a). The visual mineralization was confirmed by von Kossa staining of the same SPHs (Fig. 10b).

After 3 weeks of culture, a twofold increase in ALP level was observed for hMSCs cultured in osteogenic medium compared to hMSCs cultured in basal medium (Fig. 11a). Peak ALP levels at week 3 coincided with the start of calcium matrix production within the SPHs cultured in osteogenic medium. Deposited calcium levels were low at week 3 and increased through weeks 5 and 7 (Fig. 11b). By the fifth week, expression levels of ALP in the osteogenic samples were similar to the expression levels of ALP in basal medium samples, as would be expected with the osteogenic differentiation process.[47] All PEGDA SPHs incubated in osteogenic medium showed calcification (Fig. 12) throughout the matrices with depositions having calcium to phosphate (Ca/P) ratios ranging from 1.51 to 1.56 for all groups. The stoichiometric Ca/P ratio for pure hydroxyapatite [$Ca_{10}(PO_4)_6(OH)_2$] is 1.67. However, bone is comprised of both hydroxyapatite and calcium-deficient hydroxyapatite, thus creating a composite Ca/P ratio around 1.60 in bone.[48]

Acellular PEGDA SPHs respond to the osteogenic microenvironment by calcium deposition within the SPHs (Fig. 13). Increased levels of calcium are observed in all the acellular groups with the highest levels in unmodified PEGDA SPHs; this increase is similar to calcium levels in cellular constructs cultured in basal medium. Overall, the levels of automineralization in PEGDA SPHs by week 3 (3.15 ± 2.83 μg/mg dry weight) are much lower than those previously reported in PEGDA NPHs (28.7 ± 1.34 μg/mg dry weight for 10% PEGDA NPHs and 32.3 ± 2.50 μg/mg dry weight for 20% PEGDA NPHs)[49] for the same time frame. The acellular SPH groups also served to elucidate the contribution of stem cell–driven mineralization toward the calcium content detected within the MSC-seeded SPH groups cultured in osteogenic medium.

Discussion

The gap between the clinical demand of bone grafts and the availability of autologous and allogenic donors is widening. This has provided the incentive to find alternative techniques to promote bone formation. Bone repair by an autologous bone grafting procedure seems a

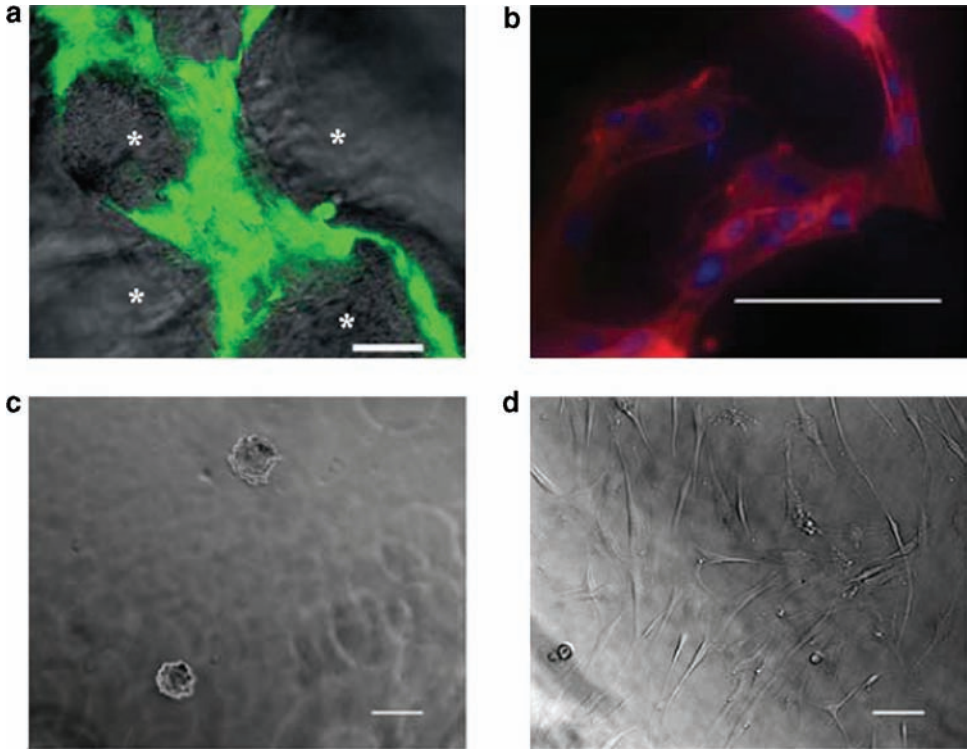

FIG. 6. (**a**) hMSCs uptake within the SPHs around the pores (*) was confirmed by staining viable hMSCs with calcein AM 7 weeks after seeding. The scale bar is 50 μm. This image was taken from a position within the center of the construct. (**b**) Actin filaments were detected using Alexa Fluor 546® phalloidin staining, and nucleus is stained with Hoechst 33258 dye, 96 h postseeding. The scale bar is 100 μm. (**c**) Light micrograph of hMSCs seeded on top of NPHs 48 h after seeding. The scale bar is 100 μm. (**d**) Light micrograph of hMSCs seeded on top of nonporous RGD-PEGDA hydrogels 48 h after seeding. The cells can be seen in their native spread morphology. The scale bar is 100 μm.

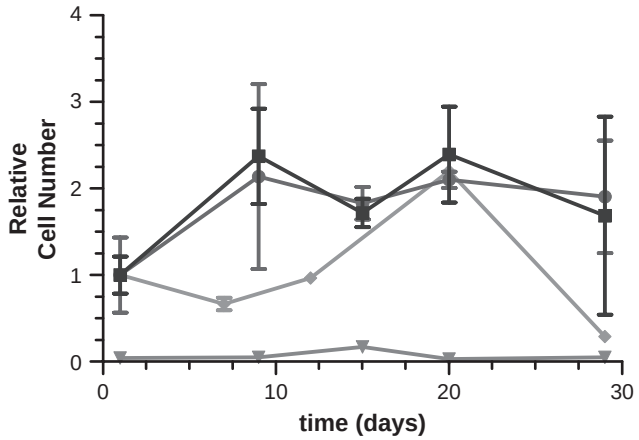

FIG. 7. hMSCs (2.5×10^5 cells) seeded in PEGDA SPH (●), in RGD-PEGDA SPH (■), on NPHs (▲), and on nonporous RGD-PEGDA hydrogels (◆) and cultured in basal medium for the period described. Cell viability assessed by the modified MTT assay and reported as a relative cell number ($n=3$; mean ± standard deviation).

promising approach because it would eliminate the shortcoming of allogenic transplants. However, tissue engineering of bone grafts requires the identification of suitable 3D osteoconductive matrix that can deliver osteoprogenitor cells. PEGDA hydrogels support MSC growth and differentiation[5,6,9,10] but have several shortcomings that limit their use *in vivo* as scaffolds for regeneration and vascularization.

SPHs have previously been synthesized using vinyl monomers by a gas foaming technique wherein gas bubbles are formed by the chemical reaction of acid and sodium bicarbonate.[44] Polymerization and foaming occur simultaneously to trap the gas bubbles within the hydrogels. This method of synthesis yields interconnected pores ranging from 100 to 600 μm that form capillary-like channels within the hydrogel.[44] With a porosity of 71 ± 2.1%, the scaffold architecture was similar to trabecular bone that has macro pores ranging in porosity from 70% to 90%.[48] The open macroporous structure of SPHs was similar to trabecular bones and also was hypothesized to allow rapid uptake of aqueous medium into the center of the dehydrated hydrogel by capillary force, thereby enabling the SPH to reach equilibrium swelling within a matter of seconds to minutes while still retaining the 3D structure of the SPH.

The rapid equilibrium swelling of the hydrogels in presence of aqueous medium enabled uptake of cell suspension without the application of any external force or mechanical device. Rapid uptake accompanied by high incorporation efficiency reduced processing time for cell seeding, an advantage over many synthetic polymeric scaffolds where prewetting or other modifications of the scaffold are required.[50] Viable cells were found distributed throughout the scaffold, indicating that the uptake by capillary-like force was not potentially harmful to the cells. Further work may be necessary to determine the specific distribution in the constructs, but this work has shown that the cells do distribute within the constructs.

After the rapid fluid uptake, the interconnected porous architecture of the 3D SPH scaffold aided in long-term survival of cells. The cells within the superporous scaffolds were found to exhibit extended cell morphology with the presence of actin filaments suggestive of attachment to extracellular matrix unlike the morphology observed in nonporous hydrogels. We currently hypothesize that these attachments are due to extracellular matrix synthesized by the cells, and we hope to confirm this in the near future. However, it is apparent that the cells have the ability to adhere within the porous PEGDA SPHs compared to their inability to adhere to unmodified NPHs.

Various research groups have previously shown the influence of different structural and shape factors, for example, nanostructures[51,52] and surface roughness,[53,54] on cell attachment to biomaterials. Poly(ethylene glycol) (PEG) microwells fabricated by soft lithography have been used as templates to initiate formation of homogenous embryoid bodies from embryonic stem cells.[55] Although PEG is considered cell repellant, the controlled microenvironment in the above system enabled high viability (>95%) of the embryoid bodies for over 10 days. Similarly, in our system, it is possible that the SPH surface coupled with the porous SPH architecture is able to promote cell adhesion to the polymer surface and later on to the matrix produced by the cells. While this aspect of the SPHs needs to be investigated further, it opens an exciting area of study where surface topography can promote MSC attachment even in the absence of cell adhesive peptides.

Not only do these cells survive short term in this architecture, but we have also shown long-term cell viability when seeded within the porous architecture of the SPH. Decreased cell viability within NPHs prepared by photopolymerization techniques has been a shortcoming, with

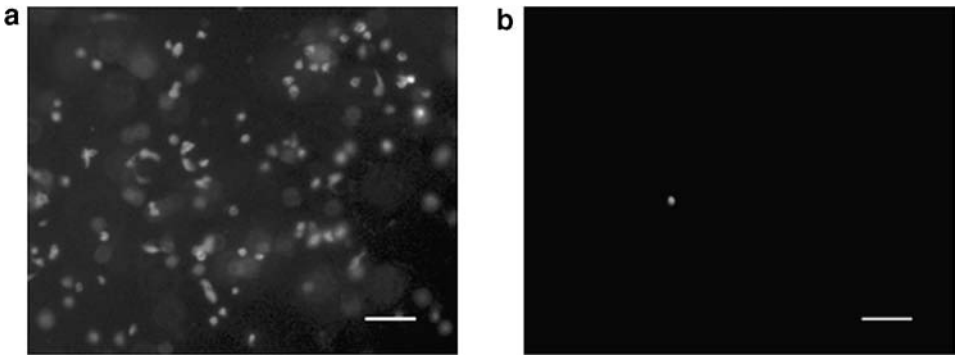

FIG. 8. Representative epifluorescent micrographs of HUVECs (2.5×10^5 cells) seeded in (**a**) RGD-PEGDA SPH and (**b**) PEGDA SPH. Viable cells (calcein AM) are present in the RGD-PEGDA SPH, but few are present in the DGR-PEGDA SPH (not shown) and PEGDA SPH. The scale bar is 100 μm in each image.

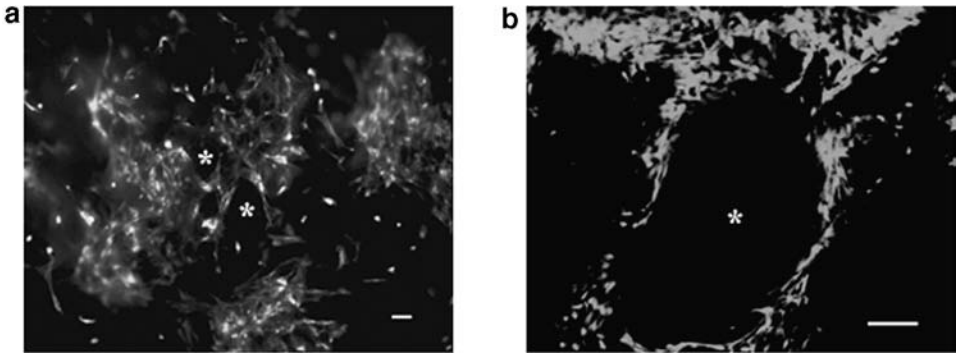

FIG. 9. Representative epifluorescent micrographs of viable hMSCs seeded in PEGDA SPHs 7 weeks postseeding. Images are representative of observed cell morphology when cultured in (**a**) basal medium and (**b**) osteogenic medium. Viable cells stained with calcein AM dye were observed on the edges of pores (*). The scale bar is 100 μm in each image.

viability dropping to around 10% of initial seeding within 4 weeks of culture when the size of the construct is larger than a few hundreds of micrometers.[12] The interconnected macroporous network of our hydrogels exposed cells seeded within the scaffold to the surrounding medium, which we hypothesize, aided in promoting long-term cell survival. Interconnected macroporous networks are also known to promote cellular ingrowth and communication influencing cell survival.[2] While the general structure of the hydrogel greatly increased cell growth, presence of cell adhesive peptides did not influence cell growth or mineralization.

Surprisingly, no difference was found in the ability of PEGDA SPHs and RGD-PEGDA SPHs to support long-term hMSC viability despite the RGD density being well above the widely accepted density required for cell adhesion.[34] The RGD peptide incorporated within the SPHs was confirmed to be in an active conformation by the adhesion of HUVECs to the RGD-PEGDA SPHs.[46] The RGD modification of PEG has been well documented to be required for cellular attachment and growth, the architecture of the SPHs itself seemed sufficient to enable MSC attachment and survival, an observation found to be cell line dependant.

At a concentration of 2.5 mM acryl-GRGDSG, no difference was observed between the unmodified PEGDA and RGD-modified PEGDA SPHs with respect to the ALP levels and the elemental content of the mineralized matrix. ALP is a cell-surface ectoenzyme that hydrolyses monophosphate esters.[56] Although its exact function is not completely clear, one of its functions is to cleave phosphate groups from biomolecules and make them available for the process of matrix mineralization. ALP activity is known to rise during the early stages of culture and peaks just before the onset of mineralization and decreases after mineralization.[56,57] In this study, the ALP levels in the constructs cultured in osteogenic medium were also found to peak at 3 weeks which coincided with the start of mineralization. By weeks 5 and 7, ALP levels dropped to the levels of constructs cultured in basal medium. Similarly, the production of calcium that was evident around week 3 increased steadily over the following weeks. At the end of the 7 weeks of culture, the PEGDA SPHs showed significantly higher levels of calcium than the RGD-PEGDA and DGR-PEGDA did. A similar effect of peptide incorporation within PEGDA-based systems and osteogenesis has been previously observed with NPHs.[29]

Modifying the PEGDA NPHs with peptides introduced single-ended crosslinking polymer chains within the system, thereby decreasing the crosslinking density and increasing the mesh size. Larger mesh sizes lead to less mineralization within the peptide modified NPHs. Although the pore sizes in our system do not vary at the macroscopic level between the three SPH groups, it is possible that increased mesh size between the crosslinked polymer chains of the peptide-modified groups has lead to lower levels of mineralization in comparison to the unmodified SPH. In addition to just the

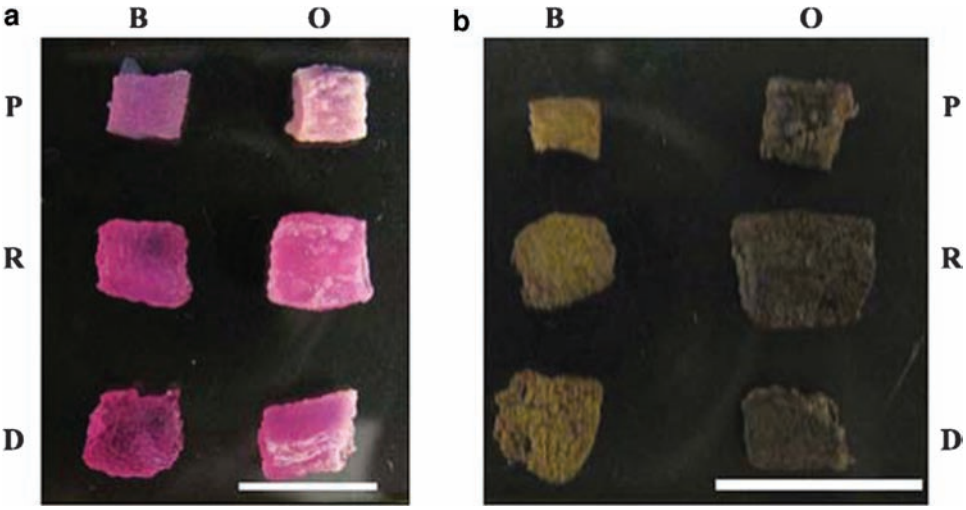

FIG. 10. PEGDA (P), RGD-PEGDA (R), and DGR-PEGDA SPHs (D) photographed after culture in basal medium (B) and osteogenic medium (O) at week 7 (**a**). Presence of calcium was confirmed by von Kossa staining (**b**) of the same SPHs. The scale bars are 1 cm. Color images available online at www.liebertonline.com/ten.

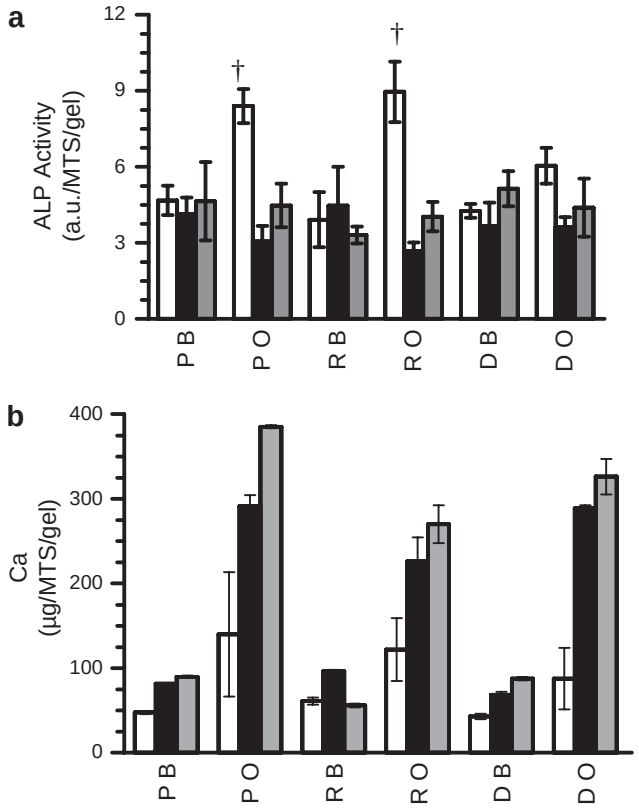

FIG. 11. (**a**) ALP levels and (**b**) calcium in serum-free medium at 3 weeks (white bars), 5 weeks (black bars), and 7 weeks (gray bars) of culture within for PEGDA (P), RGD-PEGDA (R), and DGR-PEGDA (D) SPHs cultured in (B) basal or (O) osteogenic medium, where † indicates $p < 0.01$ from the PEGDA cultured in basal medium. Calcium deposition at week 7 was higher and significantly different in the PEGDA SPHs than in the RGD-PEGDA and DGR-PEGDA as confirmed by the one-way ANOVA followed by Tukey's *post hoc* test ($p < 0.01$) ($n = 3$; mean ± standard deviation).

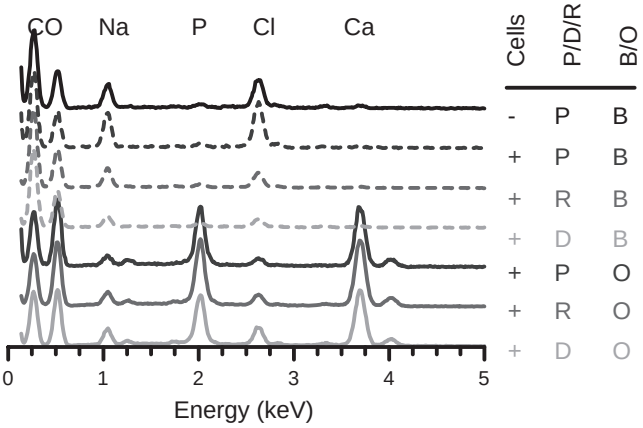

FIG. 12. Representative EDS spectra identify mineral content within PEGDA hydrogels with no cells in basal medium (−P B) PEGDA hydrogels grown in basal medium (+P B) and osteogenic medium (+P O) with cells, RGD-PEGDA hydrogels grown in basal medium (+R B) and osteogenic medium (+R O) with cells, and DGR-PEGDA grown in basal medium (+D B) and osteogenic medium (+D O) with cells.

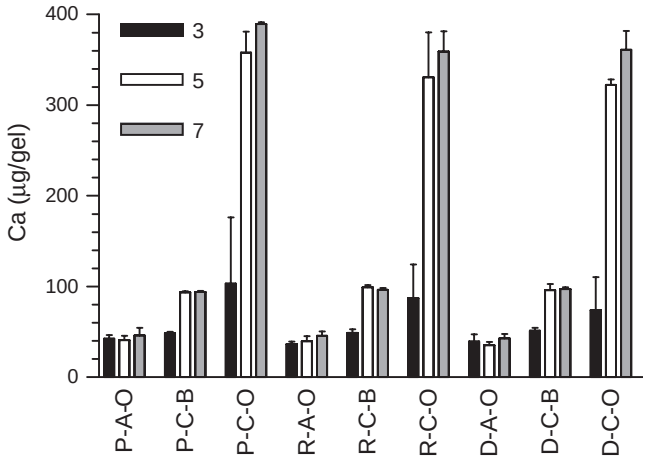

FIG. 13. (A) Acellular and (C) cellular mineralization of (P) PEGDA SPHs, (R) RGD-PEGDA, and (D) DGR-PEGDA SPHs when cultured in (O) osteogenic or (B) basal media. Calcium content calculated per gel. With the three-letter designation corresponding to the polymer composition–cellular status–medium, and P-A-O stands for acellular PEGDA SPHs incubated in osteogenic media. The samples were examined every other week beginning at (gray bars) week 3, (white bars) week 5, and (black bars) week 7 ($n = 3$; mean ± standard deviation).

mesh size effects, the mechanical properties of the hydrogels changed due to increased mesh size and peptide incorporation. The cells may be influenced by the mechanical difference between the different hydrogels. Further, the chemical differences of the peptide being present may influence the mineralization. The appropriate controls for this are included and shown that the peptide control (DGR) does not greatly differ from the test peptide (RGD). A complete study on just these effects is warranted in this system.

PEGDA-based hydrogels have been reported to exhibit automineralization upon exposure to an osteogenic microenvironment.[49,58] This is caused by the deposition of minerals such as calcium and phosphate that are absorbed from the medium and get entrapped within the nonporous gels. The mineralization tendency depends on the chemical properties of the gel and the mesh sizes of the hydrogels.[49] While phosphate-based PEGDA hydrogels are known to have higher levels of automineralization than unmodified PEGDA hydrogels,[49,58] for gels having similar chemistry, smaller mesh sizes within the construct lead to greater automineralization as smaller mesh helps in physically entrapping the calcified mineral and preventing its components from being extracted. The superporous nature of our hydrogel system might not be conducive to the initial entrapment and subsequent retention of absorbed minerals. This is an advantageous feature because the formation of a mineral ring that has been observed in case of automineralization[49] might hinder the accessibility of medium and nutrients to the cells seeded within the construct and affect long-term cell viability and function. PEGDA SPHs (no cells) and cell-seeded PEGDA SPHs, RGD-PEGDA SPHs, and DGR-PEGDA SPHs cultured in basal medium exhibited limited mineralization, and any mineral present was similar in composition to the dehydrated SPHs.

Despite the varying levels of ALP and calcium deposit across the three cellular groups, the composition of the mineralized matrix was found similar in all the three SPH groups. The atomic composition of the deposited calcium was similar to calcium-deficient hydroxyapatite, the amorphous biological precursor of bone.[48] This further supports that these scaffolds have the potential for applications in bone tissue engineering. Thus, not only were the unmodified PEGDA SPHs capable of supporting long-term stem cell viability, but they also had the potential to support stem cell–driven osteogenesis. The effect of the differentiating agents[31] caused the cells to mineralize the matrix, but the ability of the cells to populate the SPH is not well understood and must be further examined.

Conclusions

The PEGDA-based SPHs prepared in this study were capable of suspending cells in a 3D interconnected porous network and providing anchorage to cells, thus creating a biomimetic environment conducive to cell growth. Surface modifications were not essential for hMSC attachment and osteogenic mineral formation, and further investigation of this potential is warranted. The interconnected macropores within the scaffold enabled cell viability even in the core of the SPH at extended time periods. The SPHs were found not only capable of rapid uptake of hMSCs and fostering proliferation over an extended time period, but also, under the right conditions, capable of promoting hMSC mineralization with possible differentiation toward the osteoblastic lineage. Future work will examine whether differentiation has actually occurred or if the cell-driven mineralization is not differentiation related.

Given the shortcomings of current auto- and allograft tissue implants, this study provided an alternative polymer scaffold for regenerative medicine and showed that appropriate porous architecture can influence cell growth on a nonadhesive polymer scaffold. Though the idea of osteogenic mineralization by stem cells that has been explored in this study is not new, the desire for a porous biomimetic 3D scaffold that supports rapid cell uptake, cell survival, and cell differentiation is unmet, and not limited to the bone tissue alone. While the scaffolds used for the above study were cylindrical constructs, PEGDA SPHs can also be engineered in multiforms depending on the intended application. These scaffolds have great potential not only in regenerative medicine but also as model 3D systems for studying cell behavior in response to various stimuli.

Acknowledgments

The authors thank Dr. Bob Lee of the Protein Research Laboratory for the acrylated peptides, Manish K. Tiwari for assistance with MATLAB® coding, and Esha Desai and Ernest Gemeinhart for technical assistance and valuable discussions. The contribution by J.J.M. was supported by the National Institutes of Health through Grant R01 EB006261. This investigation was conducted in a facility constructed with support from Research Facilities Improvement Program Grant C06 RR15482 from the National Center for Research Resources, National Institutes of Health.

Disclosure Statement

No competing financial interests exist.

References

1. Greenwald, A.S., Boden, S.D., Goldberg, V.M., Khan, Y., Laurencin, C.T., and Rosier, R.N. Bone-graft substitutes: facts, fictions, and applications. J Bone Joint Surg Am **83-A Suppl 2 Pt 2,** 98, 2001.
2. Cowan, C.M., Soo, C., Ting, K., and Wu, B. Evolving concepts in bone tissue engineering. Curr Top Dev Biol **66,** 239, 2005.
3. Langer, R. Tissue engineering: a new field and its challenges. Pharm Res **14,** 840, 1997.
4. Peppas, N.A., Bures, P., Leobandung, W., and Ichikawa, H. Hydrogels in pharmaceutical formulations. Eur J Pharm Biopharm **50,** 27, 2000.
5. Elisseeff, J., Anseth, K., Sims, D., Mcintosh, W., Randolph, M., Yaremchuk, M., and Langer, R. Transdermal photopolymerization of poly(ethylene oxide)-based injectable hydrogels for tissue-engineered cartilage. Plast Reconstr Surg **104,** 1014, 1999.
6. Burdick, J.A., and Anseth, K.S. Photoencapsulation of osteoblasts in injectable RGD-modified PEG hydrogels for bone tissue engineering. Biomaterials **23,** 4315, 2002.
7. Hern, D.L., and Hubbell, J.A. Incorporation of adhesion peptides into nonadhesive hydrogels useful for tissue resurfacing. J Biomed Mater Res **39,** 266, 1998.
8. Hersel, U., Dahmen, C., and Kessler, H. RGD modified polymers: biomaterials for stimulated cell adhesion and beyond. Biomaterials **24,** 4385, 2003.
9. Hwang, N.S., Varghese, S., Zhang, Z., and Elisseeff, J. Chondrogenic differentiation of human embryonic stem cell-derived cells in arginine-glycine-aspartate-modified hydrogels. Tissue Eng **12,** 2695, 2006.
10. Alhadlaq, A., Tang, M., and Mao, J.J. Engineered adipose tissue from human mesenchymal stem cells maintains predefined shape and dimension: implications in soft tissue augmentation and reconstruction. Tissue Eng **11,** 556, 2005.
11. Williams, C.G., Malik, A.N., Kim, T.K., Manson, P.N., and Elisseeff, J.H. Variable cytocompatibility of six cell lines with photoinitiators used for polymerizing hydrogels and cell encapsulation. Biomaterials **26,** 1211, 2005.
12. Nuttelman, C.R., Tripodi, M.C., and Anseth, K.S. *In vitro* osteogenic differentiation of human mesenchymal stem cells photoencapsulated in PEG hydrogels. J Biomed Mater Res A **68,** 773, 2004.
13. Langer, R., and Vacanti, J.P. Tissue engineering. Science **260,** 920, 1993.
14. Crane, G.M., Ishaug, S.L., and Mikos, A.G. Bone tissue engineering. Nat Med **1,** 1322, 1995.
15. Ishaug, S.L., Crane, G.M., Miller, M.J., Yasko, A.W., Yaszemski, M.J., and Mikos, A.G. Bone formation by three-dimensional stromal osteoblast culture in biodegradable polymer scaffolds. J Biomed Mater Res **36,** 17, 1997.
16. Stosich, M.S., Bastian, B., Marion, N.W., Clark, P.A., Reilly, G., and Mao, J.J. Vascularized adipose tissue grafts from human mesenchymal stem cells with bioactive cues and microchannel conduits. Tissue Eng **13,** 2881, 2007.
17. Hutmacher, D.W. Scaffolds in tissue engineering bone and cartilage. Biomaterials **21,** 2529, 2000.
18. Gemeinhart, R.A., Park, H., and Park, K. Pore structure of superporous hydrogels. Polym Adv Technol **11,** 617, 2000.
19. Shastri, V.P., Martin, I., and Langer, R. Macroporous polymer foams by hydrocarbon templating. Proc Natl Acad Sci USA **97,** 1970, 2000.

20. Friedenstein, A.J., Chailakhjan, R.K., and Lalykina, K.S. The development of fibroblast colonies in monolayer cultures of guinea-pig bone marrow and spleen cells. Cell Tissue Kinet **3,** 393, 1970.
21. Noth, U., Osyczka, A.M., Tuli, R., Hickok, N.J., Danielson, K.G., and Tuan, R.S. Multilineage mesenchymal differentiation potential of human trabecular bone-derived cells. J Orthop Res **20,** 1060, 2002.
22. Pittenger, M.F., Mackay, A.M., Beck, S.C., Jaiswal, R.K., Douglas, R., Mosca, J.D., Moorman, M.A., Simonetti, D.W., Craig, S., and Marshak, D.R. Multilineage potential of adult human mesenchymal stem cells. Science **284,** 143, 1999.
23. Kotton, D.N., Ma, B.Y., Cardoso, W.V., Sanderson, E.A., Summer, R.S., Williams, M.C., and Fine, A. Bone marrow-derived cells as progenitors of lung alveolar epithelium. Development **128,** 5181, 2001.
24. Herrera, M.B., Bussolati, B., Bruno, S., Fonsato, V., Romanazzi, G.M., and Camussi, G. Mesenchymal stem cells contribute to the renal repair of acute tubular epithelial injury. Int J Mol Med **14,** 1035, 2004.
25. Wakitani, S., Saito, T., and Caplan, A.I. Myogenic cells derived from rat bone marrow mesenchymal stem cells exposed to 5-azacytidine. Muscle Nerve **18,** 1417, 1995.
26. Fukuda, K. Progress in myocardial regeneration and cell transplantation. Circ J **69,** 1431, 2005.
27. Phinney, D.G., and Isakova, I. Plasticity and therapeutic potential of mesenchymal stem cells in the nervous system. Curr Pharm Des **11,** 1255, 2005.
28. Arinzeh, T.L. Mesenchymal stem cells for bone repair: preclinical studies and potential orthopedic applications. Foot Ankle Clin **10,** 651, 2005.
29. Yang, F., Williams, C.G., Wang, D.A., Lee, H., Manson, P.N., and Elisseeff, J. The effect of incorporating RGD adhesive peptide in polyethylene glycol diacrylate hydrogel on osteogenesis of bone marrow stromal cells. Biomaterials **26,** 5991, 2005.
30. Bruder, S.P., Jaiswal, N., and Haynesworth, S.E. Growth kinetics, self-renewal, and the osteogenic potential of purified human mesenchymal stem cells during extensive subcultivation and following cryopreservation. J Cell Biochem **64,** 278, 1997.
31. Jaiswal, N., Haynesworth, S.E., Caplan, A.I., and Bruder, S.P. Osteogenic differentiation of purified, culture-expanded human mesenchymal stem cells *in vitro*. J Cell Biochem **64,** 295, 1997.
32. Hubbell, J.A. Biomaterials in tissue engineering. Biotechnology (NY) **13,** 565, 1995.
33. Elbert, D.L., and Hubbell, J.A. Conjugate addition reactions combined with free-radical cross-linking for the design of materials for tissue engineering. Biomacromolecules **2,** 430, 2001.
34. Massia, S.P., and Hubbell, J.A. An RGD spacing of 440 nm is sufficient for integrin alpha V beta 3-mediated fibroblast spreading and 140 nm for focal contact and stress fiber formation. J Cell Biol **114,** 1089, 1991.
35. Lichtenfels, R., Biddison, W.E., Schulz, H., Vogt, A.B., and Martin, R. CARE-LASS (calcein-release-assay), an improved fluorescence-based test system to measure cytotoxic T lymphocyte activity. J Immunol Methods **172,** 227, 1994.
36. Gaugain, B., Barbet, J., Oberlin, R., Roques, B.P., and Le Pecq, J.B. DNA bifunctional intercalators. I. Synthesis and conformational properties of an ethidium homodimer and of an acridine ethidium heterodimer. Biochemistry **17,** 5071, 1978.
37. Mosmann, T. Rapid colorimetric assay for cellular growth and survival: application to proliferation and cytotoxicity assays. J Immunol Methods **65,** 55, 1983.
38. Cooper, J.A. Effects of cytochalasin and phalloidin on actin. J Cell Biol **105,** 1473, 1987.
39. Latt, S.A., and Stetten, G. Spectral studies on 33258 Hoechst and related bisbenzimidazole dyes useful for fluorescent detection of deoxyribonucleic acid synthesis. J Histochem Cytochem **24,** 24, 1976.
40. Eaton, R.H. Plasma alkaline phosphatase assay: interconversion of results by two methods. Clin Chem **23,** 2148, 1977.
41. Woo, J., and Cannon, D.C. Metabolic intermediates and inorganic ions. In: Henry, J.B., and McPherson, R.A., ed. Clinical Diagnosis and Management by Laboratory Methods. Philadelphia, PA: WB Saunders, 1984, p. 133.
42. Sheehan, D.C., and Hrapchak, B.B. Theory and Practice of Histotechnology. St. Louis, MO: C.V. Mosby Co., 1980.
43. Ridler, T.W., and Calvard, S. Picture thresholding using an iterative selection method. IEEE Trans Sys Man Cybernet **SMC-8,** 630, 1978.
44. Gemeinhart, R.A., Chen, J., Park, H., and Park, K. pH-sensitivity of fast responsive superporous hydrogels. J Biomater Sci Polym Ed **11,** 1371, 2000.
45. Ahn, S.J., Costa, J., and Emanuel, J.R. PicoGreen quantitation of DNA: effective evaluation of samples pre- or post-PCR. Nucleic Acids Res **24,** 2623, 1996.
46. Lin, H.B., Garcia-Echeverria, C., Asakura, S., Sun, W., Mosher, D.F., and Cooper, S.L. Endothelial cell adhesion on polyurethanes containing covalently attached RGD-peptides. Biomaterials **13,** 905, 1992.
47. Lian, J.B., and Stein, G.S. Concepts of osteoblast growth and differentiation: basis for modulation of bone cell development and tissue formation. Crit Rev Oral Biol Med **3,** 269, 1992.
48. Bronzino, J. Tissue Engineering and Artificial Organs. Boca Raton, FL: CRC/Taylor & Francis, 2006.
49. Wang, D.A., Williams, C.G., Yang, F., Cher, N., Lee, H., and Elisseeff, J.H. Bioresponsive phosphoester hydrogels for bone tissue engineering. Tissue Eng **11,** 201, 2005.
50. Meinel, L., Karageorgiou, V., Fajardo, R., Snyder, B., Shinde-Patil, V., Zichner, L., Kaplan, D., Langer, R., and Vunjak-Novakovic, G. Bone tissue engineering using human mesenchymal stem cells: effects of scaffold material and medium flow. Ann Biomed Eng **32,** 112, 2004.
51. Price, R.L., Waid, M.C., Haberstroh, K.M., and Webster, T.J. Selective bone cell adhesion on formulations containing carbon nanofibers. Biomaterials **24,** 1877, 2003.
52. Savaiano, J.K., and Webster, T.J. Altered responses of chondrocytes to nanophase PLGA/nanophase titania composites. Biomaterials **25,** 1205, 2004.
53. Anselme, K., Bigerelle, M., Noel, B., Dufresne, E., Judas, D., Iost, A., and Hardouin, P. Qualitative and quantitative study of human osteoblast adhesion on materials with various surface roughnesses. J Biomed Mater Res **49,** 155, 2000.
54. Kommireddy, D.S., Sriram, S.M., Lvov, Y.M., and Mills, D.K. Stem cell attachment to layer-by-layer assembled TiO_2 nanoparticle thin films. Biomaterials **27,** 4296, 2006.

55. Karp, J.M., Yeh, J., Eng, G., and Khademhosseini, A. Controlling size, shape and homogeneity of embryoid bodies using poly(ethylene glycol) microwells. Lab Chip **7,** 786, 2007.
56. Gundberg, C.M. Biochemical markers of bone formation. Clin Lab Med **20,** 489, 2000.
57. Weinreb, M., Shinar, D., and Rodan, G.A. Different pattern of alkaline phosphatase, osteopontin, and osteocalcin expression in developing rat bone visualized by *in situ* hybridization. J Bone Miner Res **5,** 831, 1990.
58. Nuttelman, C.R., Benoit, D.S., Tripodi, M.C., and Anseth, K.S. The effect of ethylene glycol methacrylate phosphate in PEG hydrogels on mineralization and viability of encapsulated hMSCs. Biomaterials **27,** 1377, 2006.

Address correspondence to:
Richard A. Gemeinhart, Ph.D.
Department of Biopharmaceutical Sciences
College of Pharmacy
University of Illinois
833 South Wood St. (MC 865)
Chicago, IL 60612-7231

E-mail: rag@uic.edu

Received: April 21, 2008
Accepted: October 21, 2008
Online Publication Date: January 2, 2009